Large deformation numerical modeling of the short-term compression and uplift capacity of offshore shallow foundations

Published in *ASCE J. Geotechnical and Geoenvironmental Engng*. 140(3). http://dx.doi.org/10.1061/(ASCE)GT.1943-5606.000104

Santiram CHATTERJEE, M.Tech, PhD
Centre for Offshore Foundation Systems, (M053) and ARC Centre of Excellence for Geotechnical Science and Engineering,
The University of Western Australia
35 Stirling Highway, Crawley, WA – 6009, Australia
Email: santiram.chatterjee@uwa.edu.au

Divya S. K. MANA, B.Tech, M.Tech
Centre for Offshore Foundation Systems (M053) and ARC Centre of Excellence for Geotechnical Science and Engineering,
The University of Western Australia
35 Stirling Highway, Crawley, WA – 6009, Australia
Email: 20674905@student.uwa.edu.au

Susan GOURVENEC, B.Eng, PhD (corresponding author)
Centre for Offshore Foundation Systems, (M053) and ARC Centre of Excellence for Geotechnical Science and Engineering, The University of Western Australia
35 Stirling Highway, Crawley, WA – 6009, Australia
Tel: +61 8 6488 3995
Fax: +61 8 6488 1044
Email: susan.gourvenec@uwa.edu.au

Mark F. RANDOLPH, M.A., PhD
Centre for Offshore Foundation Systems, (M053) and ARC Centre of Excellence for Geotechnical Science and Engineering, The University of Western Australia
35 Stirling Highway, Crawley, WA – 6009, Australia
Email: mark.randolph@uwa.edu.au

No. of words: 4318 (introduction to conclusions inclusive)
No. of tables: 2
No. of figures: 8

ABSTRACT

Large deformation finite element analysis has been used to model the undrained response of skirted shallow foundations in uplift and compression. Large deformation effects involve changes in embedment ratio and operative local soil shear strength with increasing foundation displacement – either in tension or compression. Centrifuge model testing has shown that these changes in geometry affect the mobilized bearing capacity and the kinematic mechanisms governing failure in undrained uplift and compression. Small strain finite element analysis cannot by definition capture the effects of changing foundation embedment ratio and variation in local soil strength with foundation displacement. In this paper, load-displacement relationships, ultimate capacities and kinematic mechanisms governing failure from large deformation finite element analyses are compared with centrifuge model test results for circular skirted foundations with a range of embedment between 10 % and 50 % of the foundation diameter.

The results show that the large deformation finite element method can replicate the load-displacement response of the foundations over large displacements, pre- and post-yield, and also capture differences in the soil deformation patterns in uplift and compression. The findings from this study increase confidence in using advanced numerical methods for determining shallow skirted foundation behavior, particularly for load paths involving uplift.

INTRODUCTION

Shallow skirted foundations comprise a foundation plate that rests on the seabed with a peripheral skirt and sometimes internal skirts that penetrate into the seabed, confining a soil plug. Shallow skirted foundations are an attractive solution for many offshore applications, including fixed bottom or buoyant platforms, subsea infrastructure for wells and pipelines, and increasingly for renewable energy applications (e.g. Bye et al., 1995; Watson & Humpheson, 2007; Christophersen et al., 1992; Miller et al., 1996; Dendani & Colliat, 2002; Gaudin et al., 2011). A key advantage of skirted foundations is their ability to resist short-term tensile loads due to generation of negative excess pore pressure, also referred to as suction (relative to ambient water pressure), inside the skirt compartment during undrained pullout. Suction enables mobilization of reverse end bearing capacity i.e. a general shear failure mode as observed under compression, but in reverse. When reverse end bearing is mobilized, uplift capacity equivalent to the compression capacity is expected (Watson et al. 2000; Mana et al. 2013). In the absence of suction, uplift resistance is derived only from the frictional resistance mobilized along the skirt-soil interface, which may be up to an order of magnitude less than reverse end bearing capacity.

Several experimental studies have reported reverse end bearing of skirted foundations (Puech et al., 1993; Watson et al., 2000; Gourvenec et al., 2009, Mana et al., 2011, 2012, 2013). Experimental studies must achieve stress similitude between model and prototype conditions in order for reverse end bearing to be realized (Puech et al., 1993). As a result, model tests must be carried out in a geotechnical centrifuge which imposes constraints over the number of tests, the applied loading paths and loading sequences owing to space restrictions and hardware capability.

Numerical analysis is an attractive method of augmenting physical model programmes to consider load paths or other conditions that would be impossible or impractical to model in the centrifuge. In Total Lagrangian, i.e. small strain finite element (SSFE) analysis the nodes of the mesh move with the associated material point and all the variables are referred to the undeformed geometry. Hence SSFE analysis cannot for example, capture higher strength of deeper soil or lower strength of the shallower soil as a foundation is penetrated downwards or pulled out. In other words, SSFE analysis cannot by definition capture effects associated with changing geometry and therefore cannot distinguish between a skirted foundation in undrained compression and uplift when reverse end bearing is mobilized. Total Lagrangian analyses are also limited by gross mesh distortion or entanglement due to large movements, particularly in the finely meshed region around the skirt tip. Shortcomings of SSFE analysis to capture the kinematic failure mechanisms of shallow skirted foundations in undrained uplift and compression were explicitly illustrated by Mana et al. (2012) through comparison with centrifuge test data. The SSFE analyses were shown to represent the failure mechanisms in undrained compression reasonably but since, by definition of small strain analyses, the response in fully-bonded undrained uplift was identical but reversed in sense to that in compression, the uplift mechanisms observed in the centrifuge model tests were poorly represented.

In order to explore the full load-displacement response and any differences in failure mechanisms between undrained uplift and compression, it is important to capture the geometric and material non-linearity associated with large deformations. Numerical modeling of large deformation problems can be achieved using a finite element methodology based on the "remeshing and interpolation technique with small strain" (RITSS) approach developed by Hu & Randolph (1998a, b). This analysis technique has previously been adopted successfully to study the large displacement behavior of offshore foundations, penetrometers and pipelines (Hu et al., 1999; Zhou & Randolph, 2006, 2007; Hossain & Randolph, 2010; Wang et al., 2010a, 2010b; Chatterjee et al., 2012). To the authors' knowledge, the undrained compression and uplift responses of skirted foundations have not previously been considered by large deformation finite element (LDFE) analysis.

LDFE analysis offers the potential to augment physical modeling programmes if it can be shown that the numerical method can adequately predict the observed responses. The study presented in this paper uses LDFE analysis to back analyze centrifuge test results for circular shallow skirted foundations with a range of foundation embedment between 10 % and 50 % of the foundation diameter. The results of the LDFE analysis are compared with data from two programmes of centrifuge tests. One programme of centrifuge tests modeled a complete circular skirted foundation under undrained compression and uplift, which yielded the complete load-displacement response over large displacements (Mana et al. 2013). A second programme of centrifuge tests modeled a 'half' circular foundation that was tested against a Perspex window (Mana et al. 2012). Digital imaging and particle image velocimetry (PIV, White et al. 2003) was used to define the soil flow vectors during undrained compression and uplift enabling the kinematic mechanisms associated with failure to be identified.

LARGE DEFORMATION FINITE ELEMENT MODELING

Methodology

Remeshing and interpolation technique with small strain (RITSS, Hu & Randolph, 1998a, 1998b) falls under the category of Arbitrary Lagrangian Eulerian formulation (ALE, Ghosh & Kikuchi, 1991), in which mesh and material displacements are uncoupled to avoid severe mesh distortion in large deformation problems. In this methodology, a series of small strain Lagrangian analyses are conducted with the soil being remeshed and the stresses and material properties mapped after each small strain analysis. Recently, Wang et al. (2010a, 2010b) implemented RITSS in the commercial software Abaqus (Dassault Systèmes, 2010) due to its powerful mesh generation tools and computational efficiency. The same numerical methodology is adopted for the present study, but with some problem specific developments and modifications. The analysis procedure is carried out using a master Fortran program. Python scripts, the in-built scripting language of Abaqus, are used for pre-processing and post-processing different analyses. The master program calls various subroutines and Python scripts repeatedly, displacing the foundation incrementally, remeshing and mapping field variables between increments, until the required large displacement is achieved.

Finite element model

Fig. 1 shows a typical axisymmetric finite element model created for the LDFE analyses for a skirted foundation of diameter, D, skirt embedment depth, d, and skirt thickness, t. The foundations were modeled with prototype dimensions D = 12 m, d/D = 0.1, 0.2, 0.3 and 0.5, t/D = 0.008, replicating the foundations that were tested in the centrifuge (Mana et al. 2013). The radial extent and depth of the soil domain was defined at a distance of eight times the radius of the foundation from the center of the underside of the foundation top plate. The vertical soil boundary was restrained against radial movement and the bottom boundary was restrained against movement in radial and vertical directions. 6-node quadratic triangular axisymmetric elements from the Abaqus standard library (CAX6) were chosen for discretization of the soil. The foundation was defined as a rigid body.

The skirt-soil interface was assumed to have fully rough contact with no separation allowed in the normal direction. In practice, some reduction in shear strength may exist at the skirt-soil interface, particularly for a metallic skirt as modeled in the centrifuge tests. However, representation of partial interface roughness is impractical in the LDFE analyses. Interface elements in Abaqus cannot be prescribed constant αs_u-type strength reduction (with $0 < \alpha < 1$), so a thin layer of elements must be incorporated along the foundation-soil interface and explicitly prescribed a reduced shear strength. This method has been adopted successfully in small strain finite element analyses (e.g. Supachawarote et al., 2004; Gourvenec & Barnett, 2011; Gourvenec & Mana, 2011), but a very thin layer of a material with different properties to the rest of the continuum is impractical for large deformation analysis.

An unlimited tension interface along the underside of the foundation base plate was selected to represent the suction capacity available when a skirted foundation is fully sealed. An unlimited tension interface was also prescribed along the internal and external vertical skirt-soil interface, since, as only vertical loading was considered, tensile forces would not be transmitted to the vertical sides of the skirts and the prescribed tensile interface would not be activated. The modeled foundation parameters are summarized in Table 1.

Soil parameters

The LDFE analyses are based on a basic linear elastic perfectly plastic Tresca constitutive model with inclusion of strain rate and strain softening effects by modifying the value of undrained shear strength after each small strain step.

Einav & Randolph (2005) proposed an expression for the modified shear strength (s_u) of soil incorporating the combined effects of strain rate and strain softening given by

$$s_u = \left[1 + \mu \log\left(\frac{\max(\dot{\gamma}_{max}, \dot{\gamma}_{ref})}{\dot{\gamma}_{ref}}\right)\right]\left[\delta_{rem} + (1 - \delta_{rem})e^{-3\xi/\xi_{95}}\right]s_{ui} \quad (1)$$

where s_{ui} is the original intact shear strength at and below the reference strain rate $\dot{\gamma}_{ref}$. The first part of the equation takes account of the effect of strain rate and the second part takes account of strain softening of the soil. In Eq. (1), μ is the rate parameter or the rate of increase in strength per decade, typically taken as a value between 0.05 and 0.2 (Biscontin & Pestana, 2001; Lunne & Andersen, 2007). The maximum shear strain rate is defined as

$$\dot{\gamma}_{max} = \frac{(\Delta\varepsilon_1 - \Delta\varepsilon_3)}{\delta / D} \frac{v_f}{D} \quad (2)$$

where δ is the incremental displacement of the foundation, $\Delta\varepsilon_1$ and $\Delta\varepsilon_3$ are respectively the resulting major and minor principal strains and v_f is the foundation displacement rate. The value of reference shear strain rate may be related to laboratory values, typically from 1 % to 4 % per hour for triaxial tests and 5 to 20 % per hour for simple shear tests (Erbrich, 2005; Lunne et al., 2006; Lunne & Andersen, 2007). Here the minimum value of reference strain, $\dot{\gamma}_{ref}$ = 1 % per hour, was chosen, as has been adopted in previous numerical and analytical studies (Einav & Randolph, 2005; Zhou & Randolph, 2007; Wang et al., 2010a; Chatterjee et al., 2012). For calculation of the maximum shear strain rate, the foundation diameter D and foundation velocity v_f, were taken from the centrifuge model test conditions, a very small value of incremental foundation displacement δ = 0.0008D was selected, and $\Delta\varepsilon_1$ and $\Delta\varepsilon_3$ were extracted from the output file after each step of the analysis.

The second part of Eq. (1) accounts for the effect of softening of the soil. δ_{rem} is the reciprocal of sensitivity (S_t) of soil, i.e., the ratio of fully remolded to intact shear strength of soil. In this study, δ_{rem} was calculated from cyclic T-bar tests carried out in the centrifuge soil sample (as described in Andersen et al., 2005). ξ is the accumulated absolute plastic strain at the integration points, while ξ_{95} is the cumulative shear strain for 95 % shear strength degradation, with typical values ranging from 10 to 50 (Randolph, 2004).

Rate parameter μ and remolding parameter ξ_{95} were not ascertained for the centrifuge tests with which the LDFE analysis results are compared. These values were selected through a parametric study (described in the following section) to give good agreement with a selected centrifuge test result. The same soil parameters were applied in all the back analyses, i.e. the values of the parameters were not individually fitted for each foundation embedment ratio and load path. The selected values fall within the ranges identified in previous published studies (Biscontin & Pestana, 2001; Randolph, 2004; Einav & Randolph, 2005; Lunne & Andersen, 2007).

The best-fit linear shear strength profile measured in the centrifuge tests with the miniature T-bar penetrometer (Mana et al., 2013) was used as the base-line strength in the LDFE analyses, as defined in Table 1. Equation 1 was used to define the modified shear strength of soil after each small strain analysis step.

A value close to the undrained Poisson's ratio, ν_u = 0.49, rather than 0.5, was adopted to avoid numerical problems associated with modeling incompressible materials. The foundation and soil parameters used in the LDFE analyses are summarized in Table 1.

RESULTS

The results of the parametric LDFE analyses used to identify the input parameters used in the main programme of LDFE analyses are presented first followed by a comparison of LDFE results with centrifuge model test results defining the load-displacement response, ultimate (reverse) bearing capacity and kinematic failure mechanisms.

Parametric LDFE analyses

Parametric analyses were carried out to assess the effect of stiffness ratio, E_u/s_u, rate parameter, μ, and remolding parameter, $\xi_{95,}$ on the load-displacement response of the foundations to identify the best-fit values to represent the centrifuge test results. A single set of parameters for the LDFE analyses was selected based on best-fit with the observed load-displacement response and ultimate bearing capacity for a selected case of the foundation with embedment ratio d/D = 0.1 in undrained compression. The same parameters were used to back-analyze the response of foundations with a range of embedment ratios in both compression and uplift.

Fig. 2 a-c shows the effect of the value of E_u/s_u, μ and ξ_{95} respectively on the calculated load-displacement response and ultimate bearing capacity for the selected case of the skirted foundation with embedment ratio d/D = 0.1, with all other parameters as given in Table 1. The vertical co-ordinate is the displacement (w) of the foundation from the installation position, normalized by the foundation diameter (D). The horizontal co-ordinate defines the normalized bearing response, q_{net}/s_{u0}, with q_{net} calculated as

$$q_{net} = \frac{F}{A} - \gamma'(d + w) + \frac{W_{soilplug}}{A} \tag{3}$$

Here, F is the reaction force measured at the reference point of the foundation during compression or uplift, A is the outer cross sectional area of the skirt, γ' is the effective unit weight of soil and $W_{soilplug}$ is the weight of the soil plug inside the skirt compartment ($W_{soilplug}/A = \gamma'd$). The capacity of the foundation in uplift or compression is defined in terms of a bearing capacity factor, N_{c0}, as

$$N_{c0} = \frac{q_{net}}{s_{u0,tip}} \quad (4)$$

where $s_{u0,tip}$ is the initial shear strength at the skirt tip level.

A clear dependence of foundation response on all the parameters can be observed from Fig. 2. The bearing capacity response at low displacements is mostly affected by soil stiffness both in compression and uplift and at larger displacements by strain rate and strain softening. Increased strain rate leads to increased bearing capacity and increased remolding parameter leads to more rapid softening or hardening. Stiffness ratio E_u/s_u = 400, rate of shear strength increase per decade μ = 0.1 and cumulative shear strain for 95 % shear strength degradation ξ_{95} = 10 were selected for the full suite of LDFE analyses (see Table 1) based on good agreement with the load-displacement response in compression observed in the centrifuge for the foundation with d/D = 0.1, also included in Fig. 2.

It should be noted that, since the exact values of parameters μ and ξ_{95} were not measured for the experimental study, the values obtained through parametric study may not be a unique set. For example, the parameters will vary with the value of the foundation-soil interface roughness in order to match the observed resistance. Nonetheless, the selected values fall within expected ranges (Biscontin & Pestana, 2001; Randolph, 2004; Einav & Randolph, 2005; Lunne & Andersen, 2007) and the same set of parameters was used in all the back analyses.

Bearing response

Fig. 3 a-d compares the normalized bearing response predicted from the LDFE analyses (calculated with the input parameters given in Table 1) with observations from centrifuge tests, reported by Mana et al. (2013). Lower and upper bound solutions for rough-sided, rough-based circular foundations and $kD/s_{um} = 2$ (similar to the degree of soil heterogeneity in this study) are also shown (Martin, 2001).

Fig. 3 indicates a similar load-displacement response in compression for all the foundation embedment ratios observed in the centrifuge tests and predicted by the LDFE analyses. Resistance gradually develops until the bearing capacity is mobilized after which resistance continues to increase only in line with the increase in shear strength with further penetration. The strain rate effect dominates initially, increasing the soil bearing capacity. At larger displacements, the strain rate effect is balanced, and eventually overpowered, by the effect of soil softening due to accumulation of plastic strain. The predicted initial bearing capacities fall within the bounds of the theoretical predictions. The theoretical predictions are based on assumptions of small strain and are therefore independent of foundation displacement. In other words, only a single value of bearing capacity is predicted, corresponding to the initial embedment ratio and corresponding tip level shear strength.

The response in compression from the LDFE analyses for $d/D = 0.1$ coincides with the centrifuge test data as would be expected since this test was chosen as the selection criterion for the stiffness, rate and ductility parameters. Good agreement with the centrifuge test data is observed in the initial stiffness response in compression in the LDFE analyses with other embedment ratios. The load-displacement response is under-predicted by the LDFE analysis with increasing foundation displacement. The higher bearing resistance observed in the centrifuge tests in compression compared to that predicted by the LDFE analyses may have resulted from an increase in the operative shear strength of the soil arising from consolidation during the waiting period following installation in the centrifuge tests that was not represented in the LDFE analyses.

In uplift, resistance is gradually mobilized with increasing displacement until a peak, which is followed by (a generally) stable, but diminishing capacity as (i) embedment is lost and (ii) the foundation moves into the softer shallower soil. Beyond some critical displacement suction beneath the top plate is spontaneously lost, which corresponds to rapid loss of uplift resistance. The LDFE results over-predict the peak bearing capacity at low embedment ratio and under predict at the higher embedment ratio, d/D = 0.5 with a consistent trend of reducing over-prediction and then increasing under-prediction with increasing embedment ratio.

The LDFE analyses under-predict the rate of decrease in bearing capacity with foundation displacement following peak capacity. This is likely to be due to the fully bonded interface condition between the external skirt and soil. In reality the soil adjacent to the foundation will be pulled down as the foundation displaces upwards (by virtue of the constant volume condition) such that the loss of embedment is more severe than that due only to foundation displacement. The effect is more significant at lower embedment ratios. The proportional reduction in embedment due to downward movement is less severe with increasing initial embedment ratio.

The LDFE analyses were not able to replicate the loss of suction at the foundation-soil interface, resulting in the sudden loss of uplift resistance seen in Fig. 3a and b. The fully bonded interface between top plate and soil prescribed in the LDFE analyses ensured that unlimited suction could be maintained at any displacement.

Loss of suction was observed particularly early in the centrifuge test of the foundation with the lowest embedment ratio, d/D = 0.1. It is considered that this was due to loss of sealing in the experiment and so is not expected to be captured by the LDFE analysis.

Fig. 4 demonstrates the effect of varying stiffness, ductility and rate parameters (all other parameters being kept constant) for the foundation with embedment ratio d/D = 0.5. It is clear that a better fit can be achieved by adjusting the soil parameters. This is not necessarily unexpected since slight variations in shear strength at the different locations or time of each centrifuge test may have influenced the load-displacement response.

Bearing capacity factors

Bearing capacity factors (adopting the same terminology for uplift) predicted by the LDFE analyses and observed in the centrifuge tests are summarized in Table 2, together with the measured normalized displacements, w/D, at which the peak resistance was mobilized. In uplift, the point of failure is unambiguous. However, there is some ambiguity as to the value selected to represent compression capacity; if it is (i) the steady state value (where increase in resistance is due only to the increase in shear strength), (ii) the value at a specified foundation displacement (e.g. 5 or 10 % of the foundation diameter), or (iii) the value at the equivalent magnitude of displacement that the peak uplift resistance was mobilized. In Table 2, the bearing capacity factor in compression is taken at a fixed displacement of w/D = 0.05, by which stage the resistance has either reached a plateau or a steady increase according to the increasing shear strength with depth. Lower bound (LB) and upper bound (UB) solutions for rough-sided, rough-based circular foundations for $kD/s_{um} = 2$ (Martin, 2001) are also stated in Table 2. Similar magnitudes of bearing capacity factors were predicted by the LDFE analyses compared with the centrifuge results in both compression and uplift, with an absolute average difference of 5 %.

Bearing capacity factors predicted from SSFE analyses are also shown in Table 2. The values are identical in compression and uplift due to the small strain conditions and fully bonded foundation-soil interface. The peak bearing capacity factors predicted from the SSFE analyses are similar to those in the centrifuge tests, the LDFE analyses and the bound solutions. However, the SSFE analyses predict a constant bearing capacity with increased foundation displacement (either upwards or downwards) and cannot model the changing bearing capacity with changing foundation embedment as captured by the LDFE analyses.

Failure Mechanisms

Fig. 5a and b compare soil displacement vectors for foundations with embedment ratios d/D = 0.1 and 0.5 predicted by the LDFE analyses and observed in the half-model centrifuge tests presented by Mana et al. (2012). In uplift, even for the shallow embedment ratio of d/D = 0.1, soil around the entire foundation is mobilized rather than just the soil immediately adjacent to the skirts; indicating a general shear type reverse end bearing mechanism as opposed to a local pullout failure.

On tracing the vectors, it can be seen that while a similar volume of soil is mobilized beneath tip level at failure, different mechanisms accompany failure in compression and uplift. A Prandtl-type mechanism is evident in the displacement vectors shown in Fig. 5 for the foundations in compression whereas more of a Hill-type mechanism is evident for the foundations in uplift, particularly at low embedment. A schematic representation of Prandtl and Hill-type failures is shown in Fig. 6. A detailed discussion of the failure mechanisms observed through PIV analysis of the centrifuge tests is presented by Mana et al. (2012). The LDFE analyses capture the differences in the kinematic mechanisms in uplift and compression in line with the observed mechanisms.

The failure mechanisms can be scrutinized in more detail when presented as contours of displacement as shown in Fig. 7. The figure compares displacement contours in compression and uplift predicted by the LDFE analyses (right half) and observed from PIV analysis of the centrifuge tests (left half) for each of the skirt embedment ratios. Contours are plotted at intervals of 10 % of an incremental foundation displacement post-peak in uplift and at steady state in compression. For a given embedment ratio and load path, the contours from the LDFE analyses represent the same total foundation displacement as the contours from the equivalent PIV analysis of the centrifuge tests.

The contour plots show that the LDFE analyses predicted failure mechanisms that are broadly consistent with those observed in the centrifuge tests. An exception is the case of the deepest embedment ratio, d/D = 0.5 in compression, for which the LDFE analysis predicted a similar mechanism in compression and uplift and failed to capture the confined mechanism (i.e. not extending to the soil surface) observed in compression in the centrifuge tests. Overall, the LDFE analyses captured the differences in failure mechanism in uplift and compression for a given foundation embedment ratio.

Fig. 8 compares displacement contours between SSFE and LDFE analyses for the foundation with embedment ratio d/D = 0.1. The SSFE analyses were carried out with equivalent geometry and soil parameters to the LDFE analyses. The SSFE analyses predict identical mechanisms in compression and uplift. Differences in the response between uplift and compression cannot be captured by small strain finite element analysis since the geometry of the mesh is not updated and therefore the response in (fully bonded) uplift is by definition identical in nature to that in compression. Also, the Prandtl-type mechanism observed in compression in the centrifuge tests and the LDFE analysis is not evident in the SSFE result.

CONCLUDING REMARKS

This paper has demonstrated the potential of large deformation finite element (LDFE) analysis as a tool to predict the bearing response of shallow skirted foundations under undrained compression and uplift. LDFE analysis was used to back analyze centrifuge tests on shallow skirted foundations with a range of embedment ratios. The predicted response showed good agreement in terms of both predicted bearing capacity factor and failure mechanism.

The LDFE analyses predicted the full load-displacement response, pre- and post-yield. Changes in bearing capacity with foundation displacement were predicted, resulting from changing embedment ratio and local shear strength. Small strain analyses cannot capture this phenomenon in a single analysis. The LDFE analyses under-predicted the rate of change of bearing capacity with foundation displacement in uplift for low foundation embedment ratios. This is considered to be a result of the fully bonded skirt-soil interface underestimating the downward movement of the soil adjacent to the foundation skirt as the foundation displaces upwards. This downward movement increases the loss of embedment beyond that simply from foundation displacement, increasing the rate of reduction of bearing capacity with foundation displacement.

LDFE analyses were able to capture differences in failure mechanisms in undrained uplift and compression as observed from PIV analysis of centrifuge tests – a feature that cannot be captured by small strain finite element analyses.

The analyses reported in this paper have shown that LDFE techniques, coupled with an appropriate soil model, can capture the complete load-displacement behavior and kinematic failure mechanisms observed during large movements of skirted foundations in undrained compression and uplift. The results presented increase confidence in using LDFE analysis to augment experimental test programmes to enable load paths or other site specific conditions to be considered that would be impossible or impractical to model experimentally.

ACKNOWLEDGEMENTS

The work described here forms part of the activities of the Centre for Offshore Foundation Systems, currently supported as a node of the Australian Research Council Centre of Excellence for Geotechnical Science and Engineering and the Lloyds Register Foundation. The work presented in this paper was supported through ARC grant DP0988904. This support is gratefully acknowledged.

REFERENCES

Andersen, K.H., Murff, J.D., Randolph, M.F., Clukey, E.C., Erbrich, C.T., Jostad, H.P., Hansen, B., Aubeny, C., Sharma, P., and Supachawarote, C. (2005). “Suction anchors for deepwater applications.” *Proc. 1st Int. Symp. Frontiers in Offshore Geotechnics (ISFOG)*, Perth, Australia, 1-30.

Biscontin, G., and Pestana, J. M. (2001). “Influence of peripheral velocity on vane shear strength of an artificial clay.” *Geotech. Test. J.*, 24(4), 423-429.

Bye, A., Erbrich, C., Rognlien, B., and Tjelta, T.I. (1995). “Geotechnical design of bucket foundations.” *Proc. Annual Offshore Technology Conf.,* Houston, OTC 7793.

Chatterjee, S., Randolph, M. F., and White, D. J. (2012). “The effects of penetration rate and strain softening on the vertical penetration resistance of seabed pipelines.” *Géotechnique*, 62(7), 573-582.

Christophersen, H.P., Bysveen, S., and Stϕve, O.J. (1992). “Innovative Foundation Systems Selected for the Snorre Field Development.” *Proc. 6th International Conference on the Behavior of Offshore Structures (BOSS)*, 1, 81-94.

Dassault Systèmes (2010). “*Abaqus analysis users’ manual.*” Simula Corp, Providence, RI, USA.

Dendani, H., and Colliat, J-L. (2002). “Girassol: design analyses and installation of the suction anchors.” *Proc. Annual Offshore Tech. Conf.*, Houston, OTC 14209.

Einav, I., and Randolph, M. F. (2005). “Combining upper bound and strain path methods for evaluating penetration resistance.” *Int. J. Numer. Methods Eng.*, 63(14), 1991- 2016.

Erbrich, C. T. (2005). “Australian frontiers – spudcans on the edge.” *Proc. 1st Int. Symp. on Frontiers in Offshore Geotechnics*, Perth, 49-74.

Gaudin, C., Mohr, H., Cassidy, M. J., Bienen, B., and Purwana, O. A. (2011). “Centrifuge experiments of a hybrid foundation under combined loading.” *Proc. 21st Int. Off. Pol. Engng. Conf. (ISOPE)*, Hawaii, USA.

Ghosh, S., and Kikuchi, N. (1991). “An arbitrary Lagrangian-Eulerian finite element method for large deformation analysis of elastic-viscoplastic solids.” *Comput. Methods Appl. Mech. Eng.* 86(2), 127-188.

Gourvenec, S. M., Acosta-Martinez, H. E., and Randolph, M. F. (2009). “Experimental study of uplift resistance of shallow skirted foundations in clay under transient and sustained concentric loading.” *Géotechnique*, 59(6), 525-537.

Gourvenec, S., and Barnett, S. (2011). "Undrained failure envelope for skirted foundations under general loading." *Géotechnique*, 61(3), 263-270.

Gourvenec, S., and Mana, D. S. K. (2011). "Undrained vertical bearing capacity factors for shallow foundations." *Géotechnique Letters*, 1(4), 101-108.

Hossain, M. S., and Randolph, M. F. (2010). "Deep-penetrating spudcan foundations on layered clays: numerical analysis." *Géotechnique* 60**(**3), 171–184.

Hu, Y., and Randolph, M. F. (1998a). "A practical numerical approach for large deformation problems in soil." *Int. J. Numer. Analyt. Meth. Geomech.*, 22**(**5), 327-350.

Hu, Y., and Randolph, M. F. (1998b). "*H*-adaptive FE analysis of elastoplastic nonhomogeneous soil with large deformation." *Comput. Geotech.* 23(1-2), 61-83.

Hu, Y., Randolph, M. F., and Watson, P. G. (1999). "Bearing response of skirted foundation on nonhomogeneous soil." J. Geotech. Geoenviron. Engng, ASCE, 125(11), 924-935.

Lunne, T., Berre, T., Andersen, K. H., Strandvik, S., and Sjursen, M. (2006). "Effects of sample disturbance and consolidation procedures on measured shear strength of soft marine Norwegian clays." *Can. Geotech. J.*, 43(7), 726- 750.

Lunne, T., and Andersen, K. H. (2007). "Soft clay shear strength parameters for deepwater geotechnical design." *Proc. 6th Int. Offshore Site Investigation and Geotechnics Conf.: Confronting New Challenges and Sharing Knowledge*, Society for Underwater Technology, London, 1, 151-176.

Mana, D. S. K., Gourvenec, S. M., Hossain, M. S., and Randolph, M. F (2011). "Experimental investigation of the undrained response of a shallow skirted foundation subjected to vertical compression and uplift." *Proc. 30th Int. Conf.*

Ocean Off. Arctic Engng (OMAE), Rotterdam, The Netherlands, OMAE2011-49072, 771-778.

Mana, D. S. K., Gourvenec, S. M., Randolph, M. F., and Hossain, M. S. (2012). “Failure mechanisms of skirted foundations in uplift and compression.” *Int. J. Phy. Mod. Geotech. (IJPMG)*, 12(2), 47-62.

Mana, D. S. K., Gourvenec, S. M., and Randolph, M. F. (2013). “An experimental investigation of reverse end bearing of offshore shallow foundations.” *Canadian Geotechnical Journal*, *doi:10.1139/cgj-2012-0428.*

Martin, C. M. (2001). “Vertical bearing capacity of skirted circular foundations on Tresca soil.” *Proc. 15th Int. Conf. on Soil Mechanics and Geotechnical Engineering*, Istanbul, 1, 743-746.

Miller, D. M., Frazer, I., and Brevig, P. (1996). “The Heidrun Field – Marine Operations.” *Proc. Annual Offshore Technology Conf.*, Houston, OTC 8101.

Puech, A., Iorio, J.-P., Garnier, J., and Foray, P. (1993). “Experimental study of suction effects under mudmat type foundations.” *Proc. Canadian Conference on Marine Geotechnical Engineering*. St. John's, Newfoundland, 3**,** 1062-1080.

Randolph, M. F. (2004). “Characterization of soft sediments for offshore applications. Keynote Lecture.” *Proc. 2nd Int. Conf. on Site Characterization*, Porto, Portugal, 1, Millpress Science Publishers, Rotterdam, 209-231.

Supachawarote, C., Randolph, M. F., and Gourvenec, S. (2004). “Inclined pullout capacity of suction caissons.” *Proc. 14th Int. Offshore and Polar Eng. Conf.*, Toulon, France, 500-506.

Wang, D., White, D. J., and Randolph, M. F. (2010a). “Large deformation finite element analysis of pipe penetration and large-amplitude lateral displacement.” *Can. Geotech. J.*, 47(8), 842-856.

Wang, D., Hu, Y., and Randolph, M. F. (2010b). "Three-dimensional large deformation finite-element analysis of plate anchors in uniform clay." *J. Geotech. Geoenviron. Engng, ASCE*, 136(2), 355-365.

Watson, P. G., Randolph, M. F., and Bransby, M. F (2000). "Combined lateral and vertical loading of caisson foundations." *Proc. Annual Offshore Technology Conf.*, Houston, OTC 12195.

Watson. P. G., and Humpheson, C. (2007). "Foundation design and installation of the Yolla-A platform." *Proc. 6th Int. Offshore Site Investigation and Geotechnics Conf. Soc. for Underwater Technology*, London, UK, 399-412.

White, D. J., Take, W. A., and Bolton, M. D. (2003). "Soil deformation measurement using Particle Image Velocimetry (PIV) and photogrammetry." *Géotechnique*, 53(7), 619-631.

Zhou, H., and Randolph, M. F. (2006). "Large deformation analysis of suction caisson installation in clay." *Can. Geotech. J.* 43(12), 1344-1357.

Zhou, H., and Randolph, M. F. (2007). "Computational techniques and shear band development for cylindrical and spherical penetrometers in strain-softening clay." Int. J. Geomech., 7(4), 287-295.

Table 1. Parameters used in LDFE analysis

Parameters	**Values**
Foundation:	
Foundation diameter, D	12 m
Skirt embedment depths, d	1.2 m, 2.4 m, 3.6 m & 6 m (d/D = 0.1, 0.2, 0.3 & 0.5)
Skirt wall thickness, t	0.1 m (t/D = 0.008)
Skirt-soil interface	Fully rough
Soil:	
Shear strength of soil at mudline, s_{um}	7.0 kPa
Shear strength gradient, k	1.3 kPa/m
Submerged unit weight of soil, γ'	7.0 kN/m^3
Stiffness ratio, E_u/s_u	400 (100 & 1000)
Poisson's ratio, ν_u	0.49
Strain rate and softening:	
Reference shear strain rate, $\dot{\gamma}_{ref}$	3 x 10^{-6} s^{-1}
Vertical skirt penetration rate, v_f	0.0001 m/s
Incremental foundation displacement, δ	0.08 % D
Rate of strength increase per decade, μ	0.1
Sensitivity of clay, S_t	2.7
Accumulated plastic strain at which 95 % soil strength reduction occurs by remolding, ξ_{95}	10

Table 2. Summary of bearing capacity factors from centrifuge tests and LDFE analysis compared with SSFE analysis and the theoretical solutions given by Martin (2001)

d/D	Bearing capacity factor, N_{c0}						
	Compression*				Uplift (w/D)		SSFE
	Centrifuge	LDFE	LB	UB	Centrifuge	LDFE	
0.1	9.17	9.24	8.05	9.50	8.00 (0.020)	8.88 (0.024)	8.8
0.2	10.18	9.63	8.50	10.50	9.30 (0.030)	9.33 (0.034)	9.55
0.3	10.67	9.92	8.90	11.05	9.80 (0.045)	9.62 (0.040)	10.1
0.5	11.38	10.18	9.45	12.50	10.85 (0.047)	10.03 (0.048)	10.9

***Compression capacity taken at a displacement w/D = 0.05 at which point a steady state had been reached.**

List of figure captions

Fig. 1. Finite element mesh used in LDFE analysis

Fig. 2. Variation of bearing capacity results with variation of (a) stiffness ratio E_u/s_u (b) strain rate parameter μ and (c) softening parameter ξ_{95} (all other parameters as in Table 1) for d/D = 0.1

Fig. 3. (a ~ d) Comparison of bearing capacity factors for embedment ratios d/D = 0.1, 0.2, 0.3 and 0.5 from LDFE and centrifuge tests

Fig. 4 Comparison of resistances between LDFE and centrifuge tests for d/D = 0.5: (a) E_u/s_u = 500; (b) ξ_{95} = 50; (c) μ = 0.2

Fig. 5. Comparison of the displacement vectors for embedment ratios 0.1 & 0.5 from LDFE and PIV analyses

Fig. 6 Difference in failure mechanism in compression and uplift

Fig. 7. Comparison of the normalized displacement contours from PIV and LDFE analyses

Fig. 8. Comparison of failure mechanisms predicted by SSFE and LDFE analyses (d/D = 0.1): (a) Compression; (b) Uplift

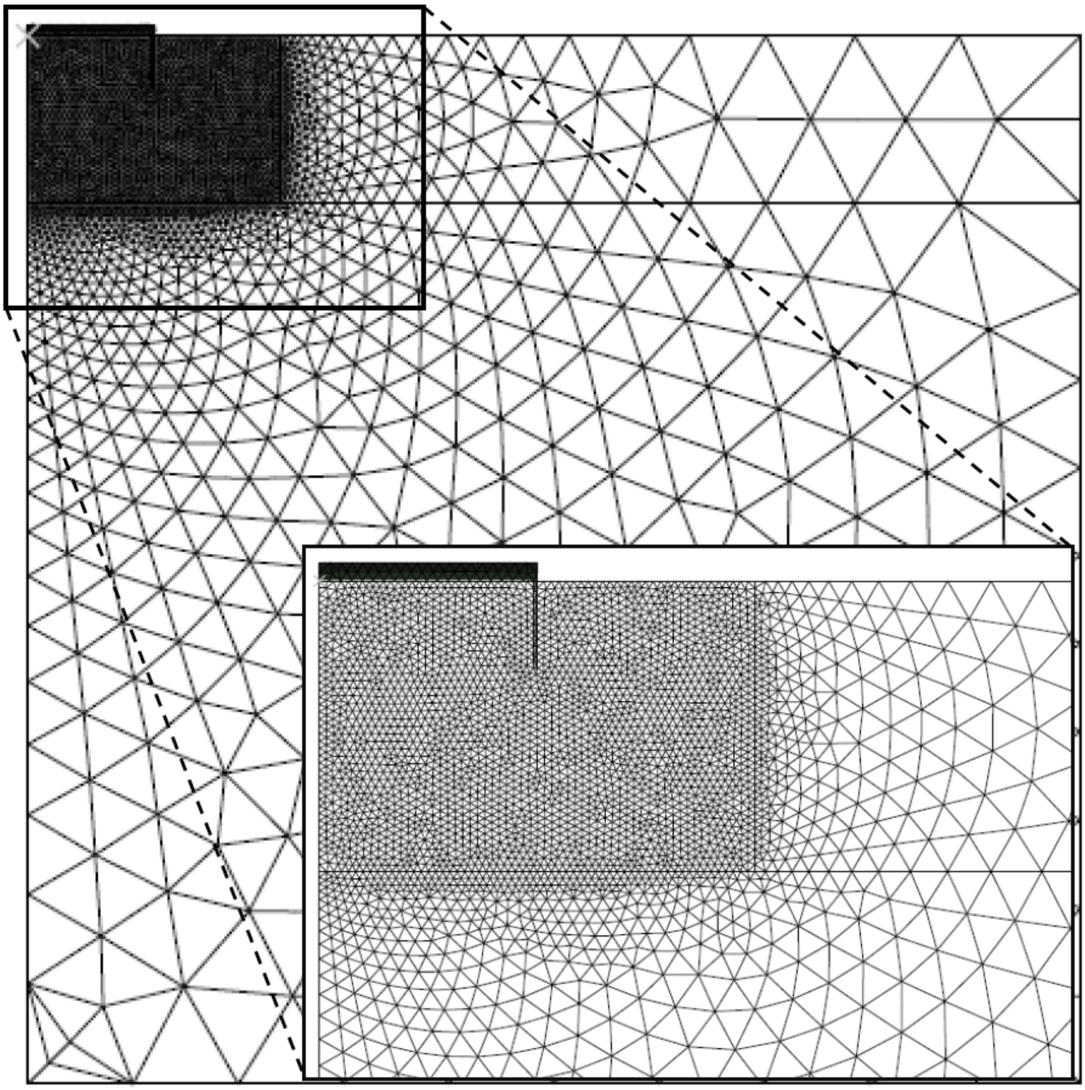

Fig. 1. Finite element mesh used in LDFE analysis

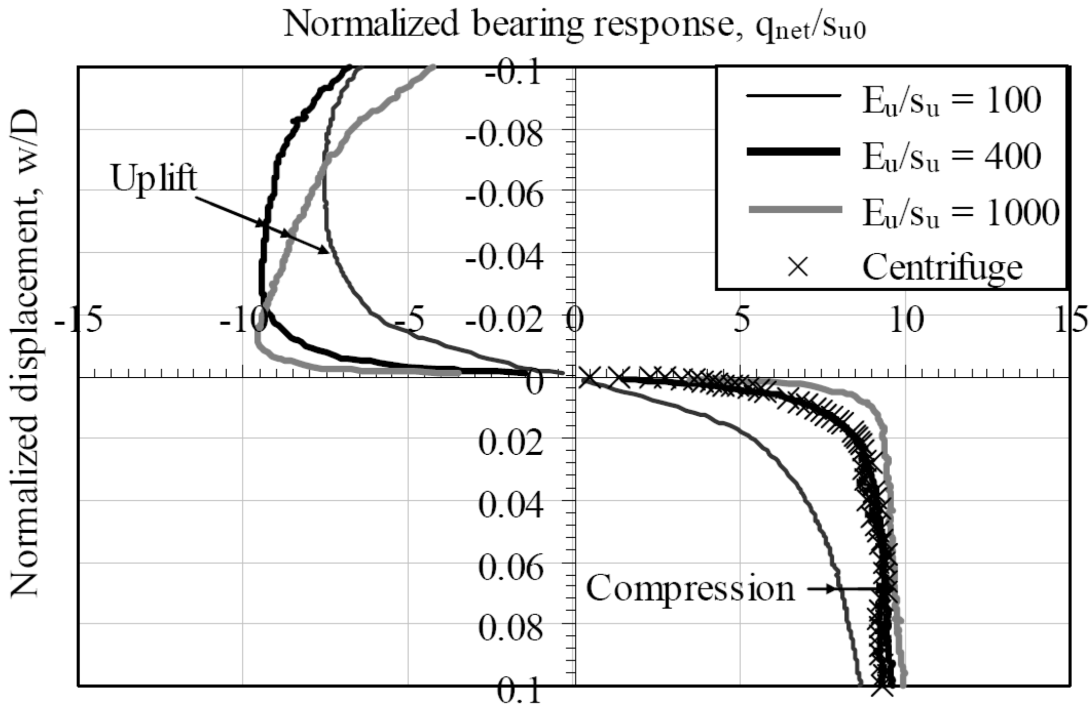

Normalized bearing response, q_{net}/s_{u0}
Normalized displacement, w/D
E_u/s_u = 100
E_u/s_u = 400
E_u/s_u = 1000
Centrifuge
Uplift
Compression
-15
-10
-5
0
5
10
15
-0.1
-0.08
-0.06
-0.04
-0.02
0
0.02
0.04
0.06
0.08
0.1

(a)

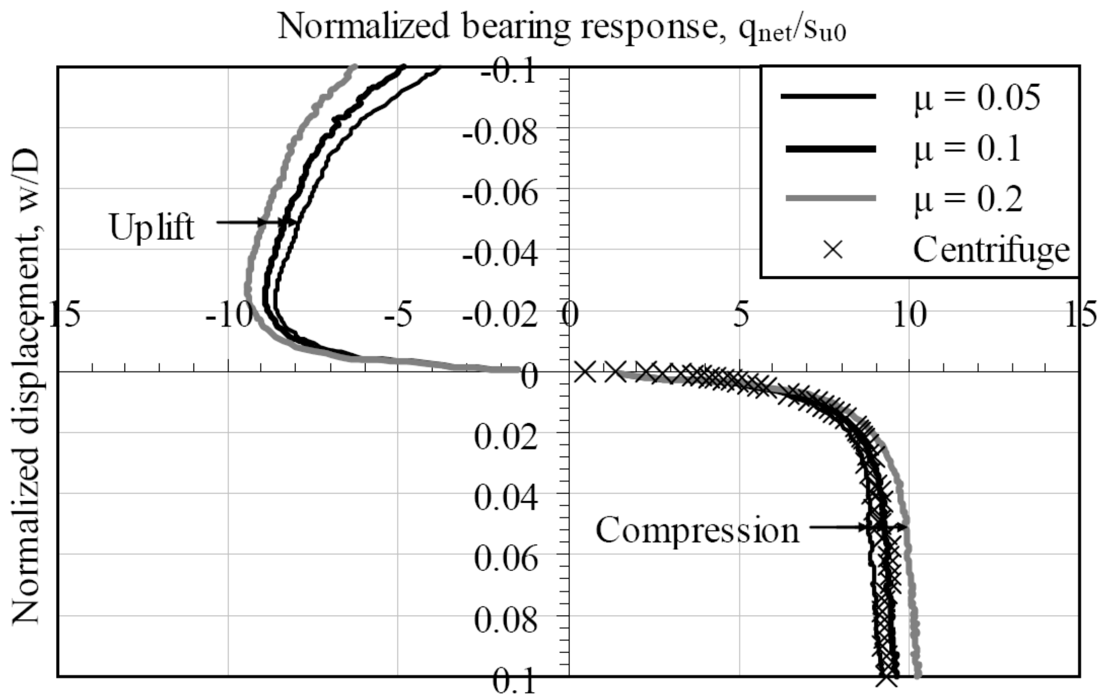

Normalized bearing response, q_{net}/s_{u0}
Normalized displacement, w/D
μ = 0.05
μ = 0.1
μ = 0.2
Centrifuge
Uplift
Compression
-15
-10
-5
0
5
10
15
-0.1
-0.08
-0.06
-0.04
-0.02
0
0.02
0.04
0.06
0.08
0.1

(b)

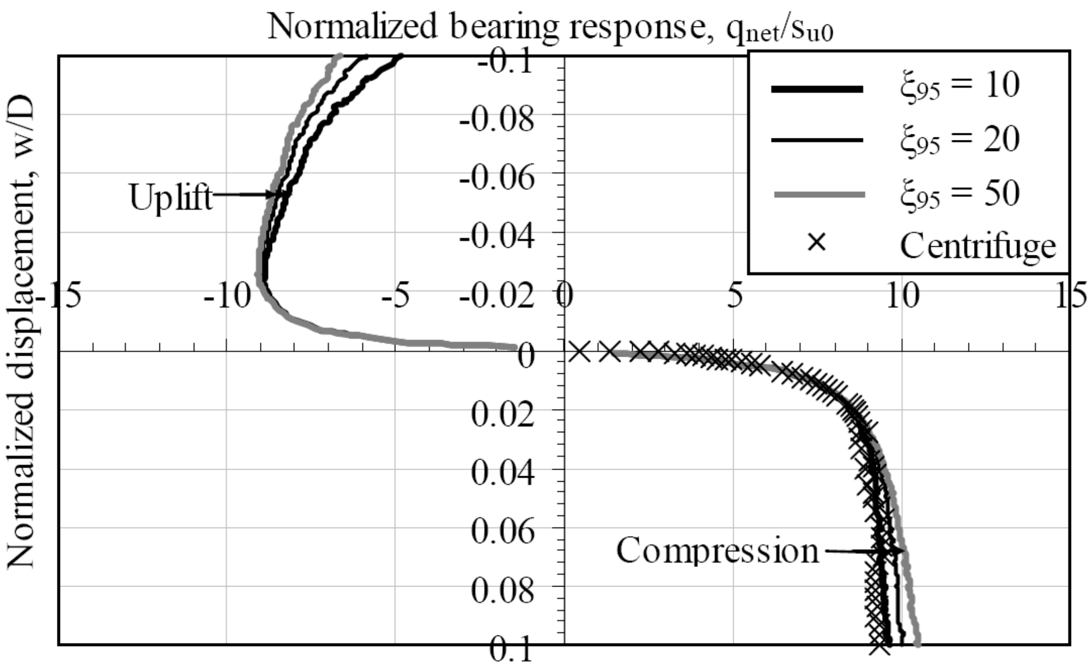

(c)

Fig. 2. Variation of bearing capacity results with variation of (a) stiffness ratio E_u/s_u (b) strain rate parameter μ and (c) softening parameter ξ_{95} (all other parameters as in Table 1) for d/D = 0.1

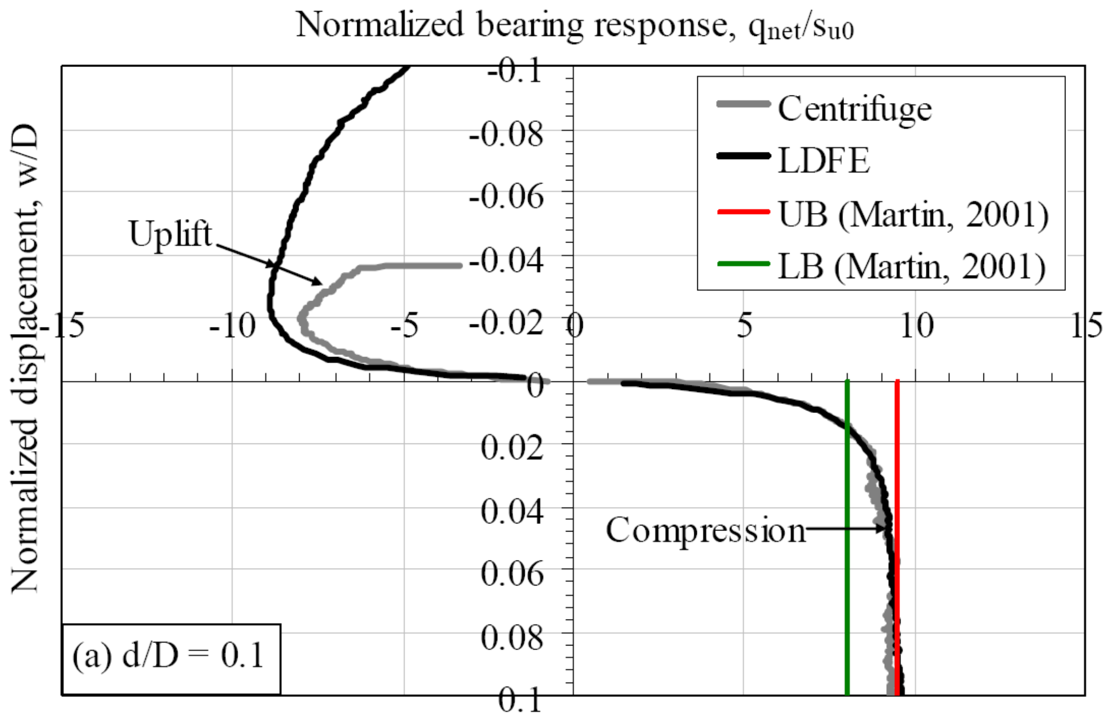
Normalized bearing response, qnet/su0
Normalized displacement, w/D
Centrifuge
LDFE
UB (Martin, 2001)
LB (Martin, 2001)
Uplift
Compression
(a) d/D = 0.1
-15
-10
-5
0
5
10
15
-0.1
-0.08
-0.06
-0.04
-0.02
0
0.02
0.04
0.06
0.08
0.1

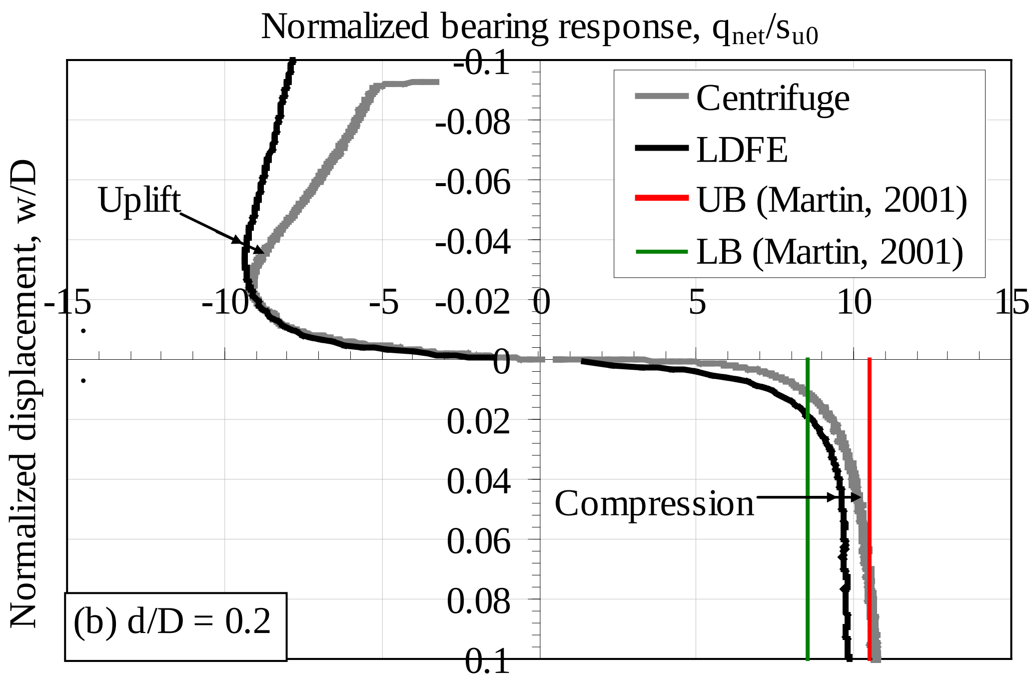
Normalized bearing response, qnet/su0
Normalized displacement, w/D
Centrifuge
LDFE
UB (Martin, 2001)
LB (Martin, 2001)
Uplift
Compression
(b) d/D = 0.2
-15
-10
-5
0
5
10
15
-0.1
-0.08
-0.06
-0.04
-0.02
0
0.02
0.04
0.06
0.08
0.1

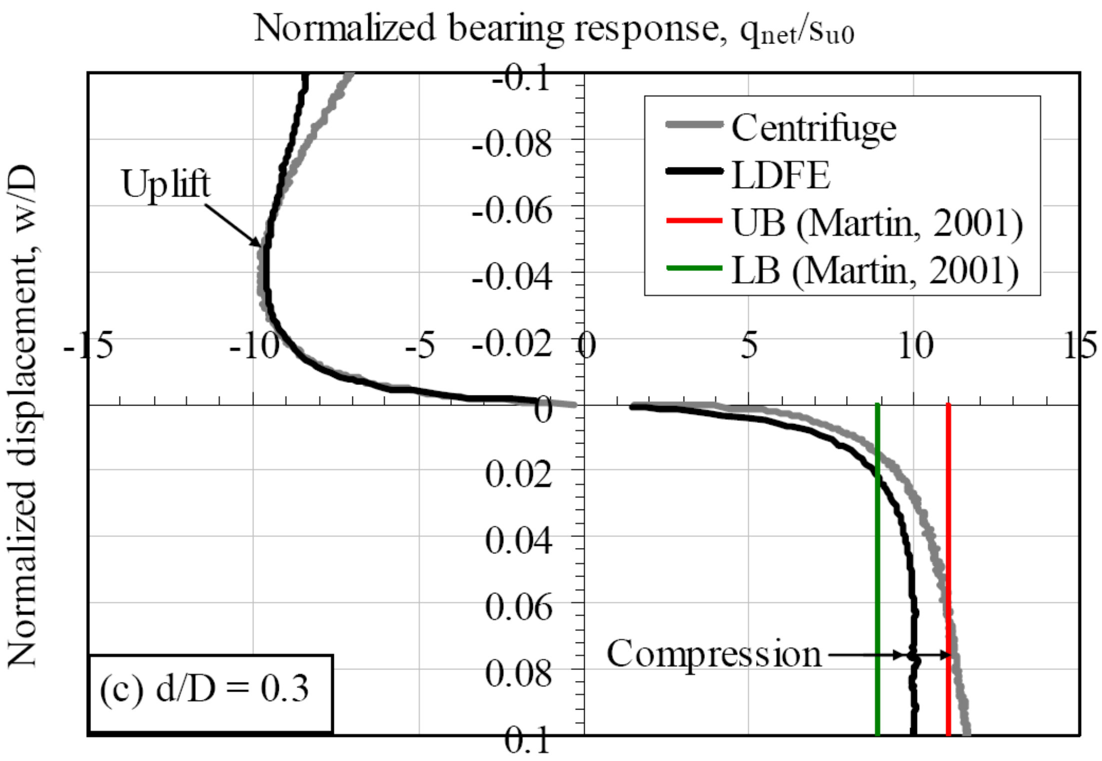

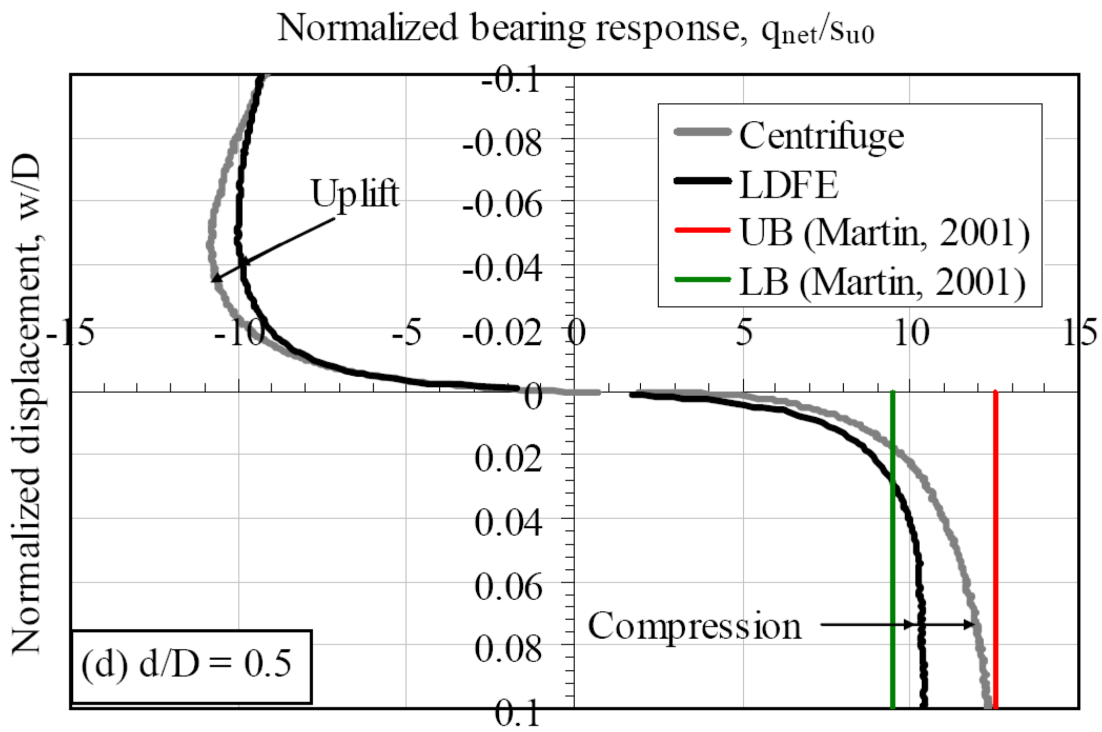

Fig. 3. (a ~ d) Comparison of bearing capacity factors for embedment ratios d/D = 0.1, 0.2, 0.3 and 0.5 from LDFE and centrifuge tests

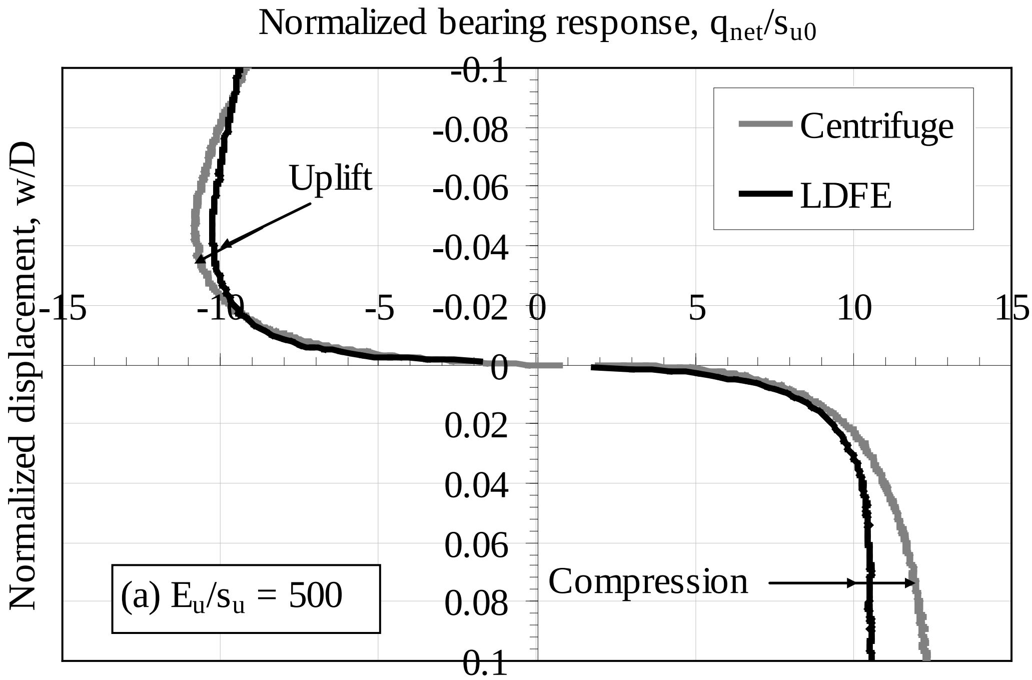
Normalized bearing response, q_{net}/s_{u0}
Normalized displacement, w/D
Centrifuge
LDFE
Uplift
Compression
(a) E_u/s_u = 500
-15
-10
-5
0
5
10
15
-0.1
-0.08
-0.06
-0.04
-0.02
0
0.02
0.04
0.06
0.08
0.1

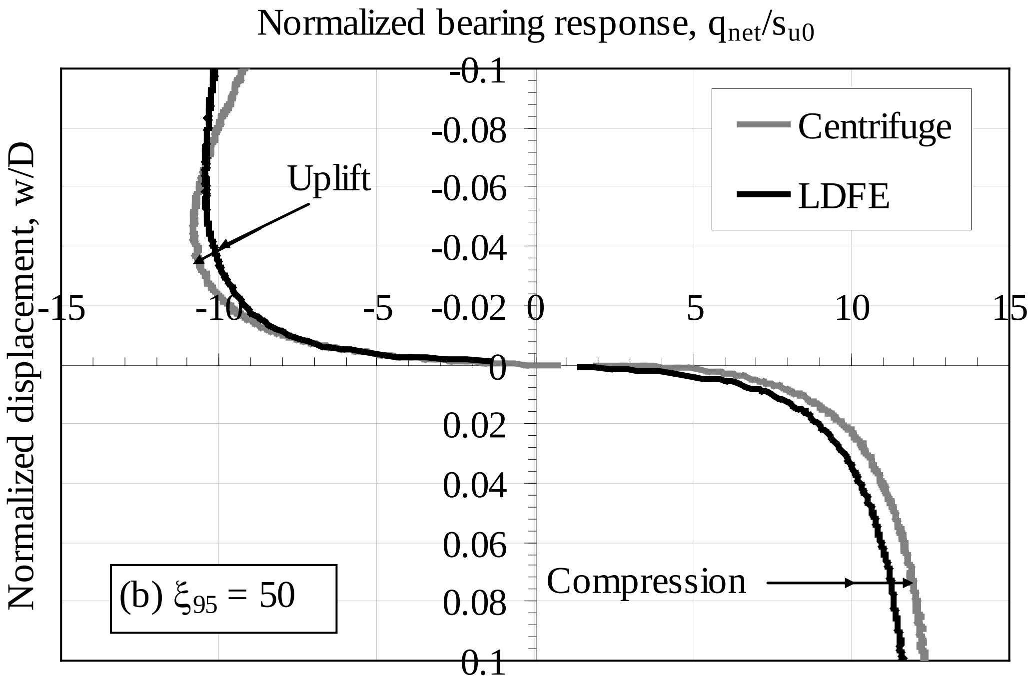
Normalized bearing response, q_{net}/s_{u0}
Normalized displacement, w/D
Centrifuge
LDFE
Uplift
Compression
(b) ξ_{95} = 50
-15
-10
-5
0
5
10
15
-0.1
-0.08
-0.06
-0.04
-0.02
0
0.02
0.04
0.06
0.08
0.1

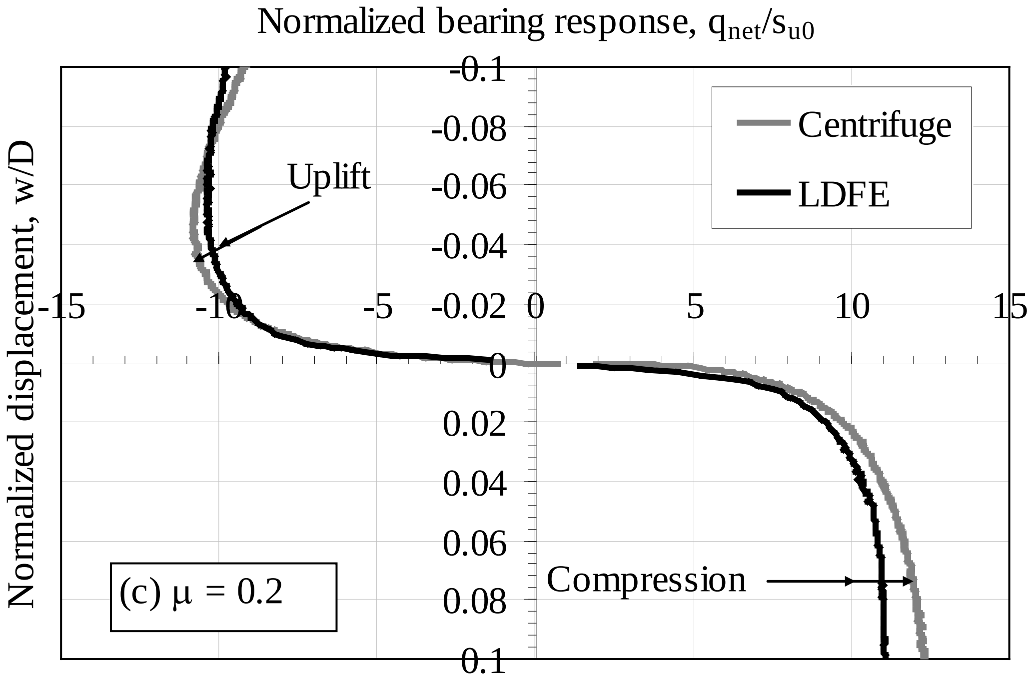

Fig. 4 Comparison of resistances between LDFE and centrifuge tests for d/D = 0.5: (a) E_u/s_u = 500; (b) ξ_{95} = 50; (c) μ = 0.2

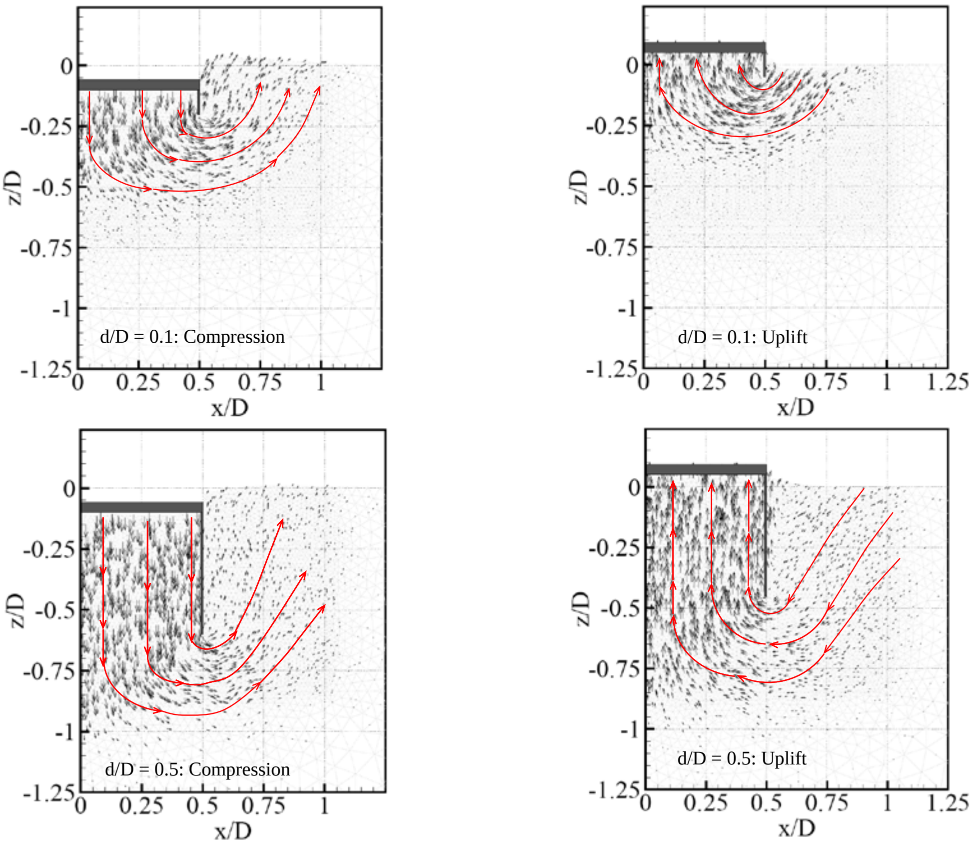

(a) LDFE analysis

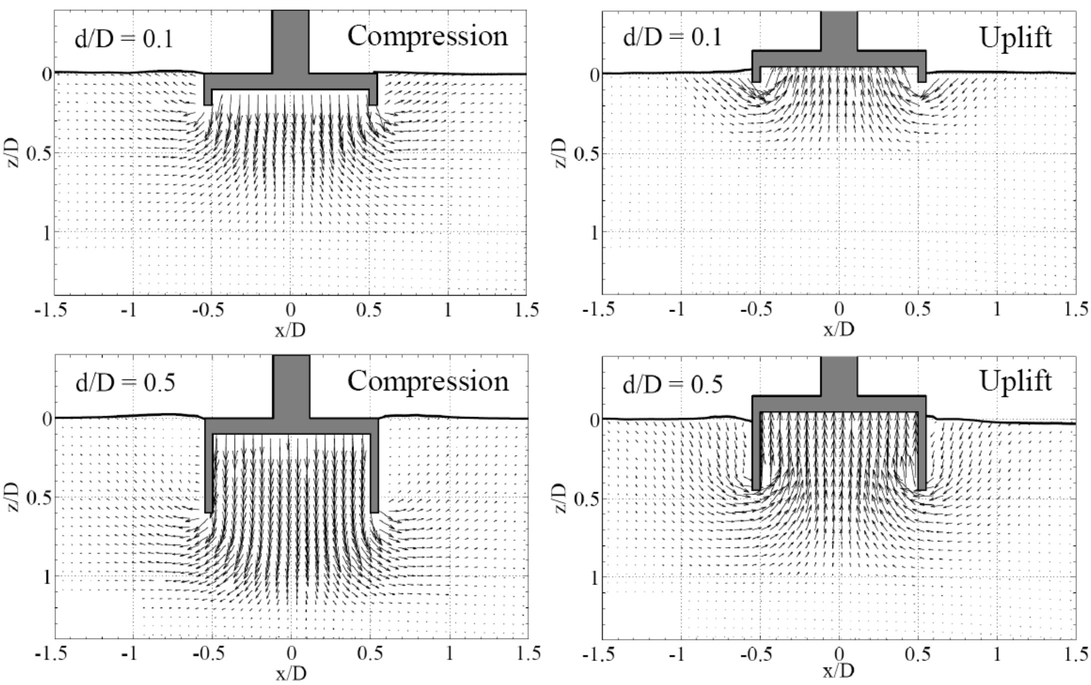

(b) PIV analysis

Fig. 5. Comparison of the displacement vectors for embedment ratios 0.1 & 0.5 from LDFE and PIV analyses

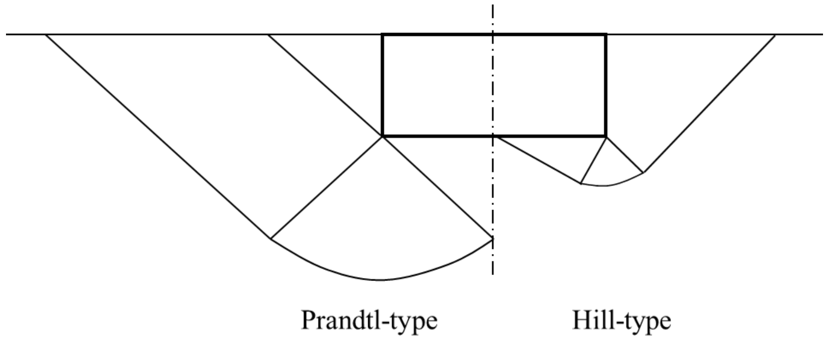

Fig. 6 Difference in failure mechanism in compression and uplift

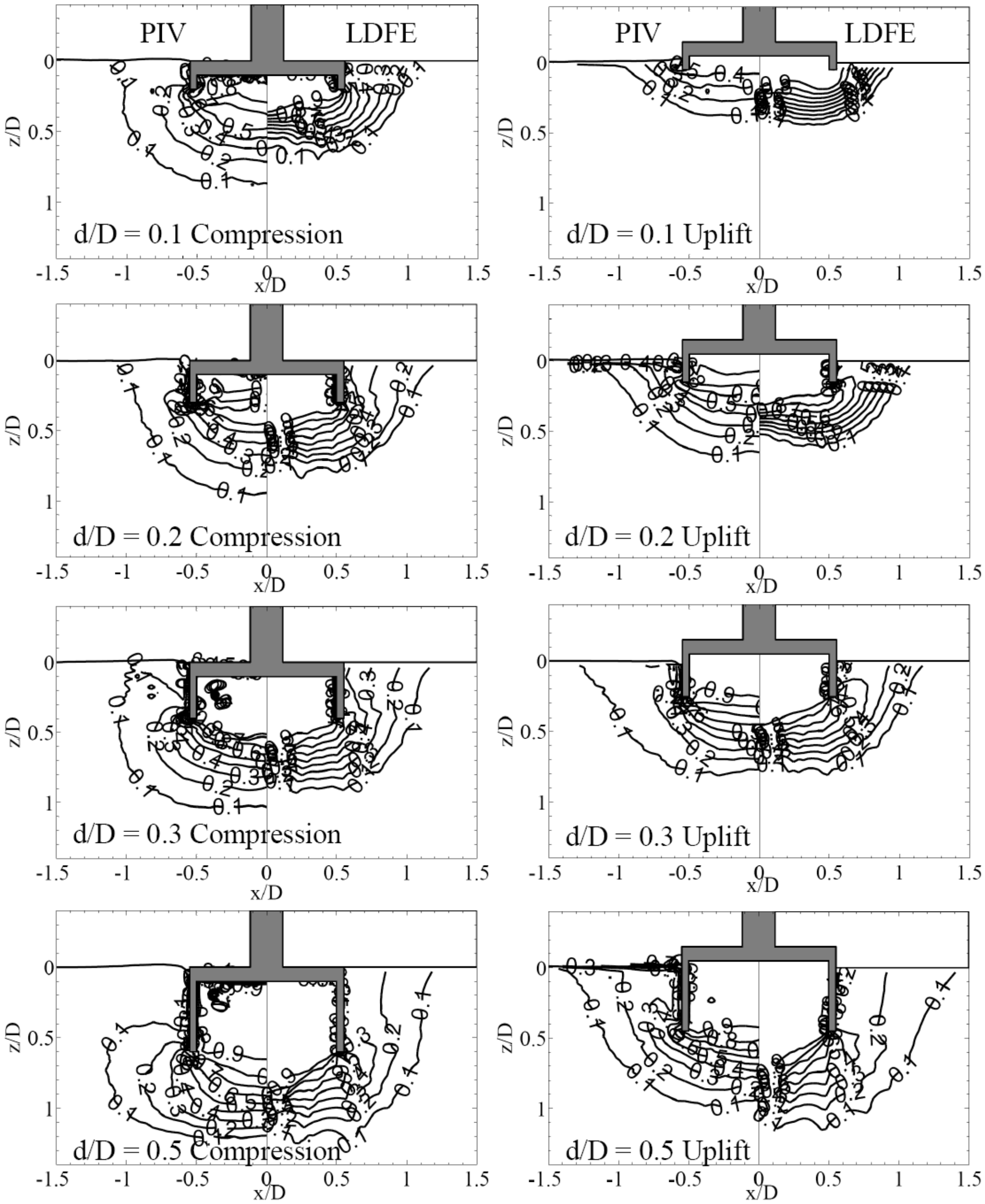

Fig. 7. Comparison of the normalized displacement contours from PIV and LDFE analyses

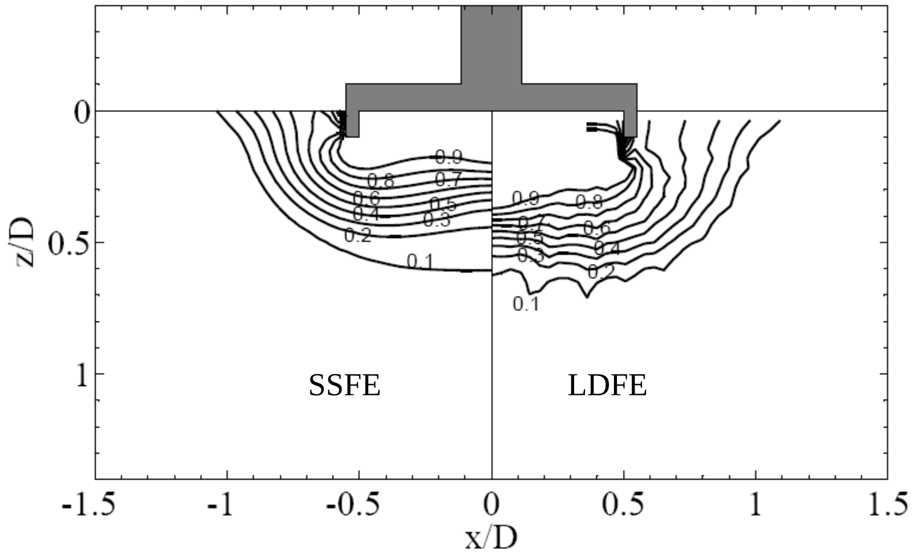

(a) Compression

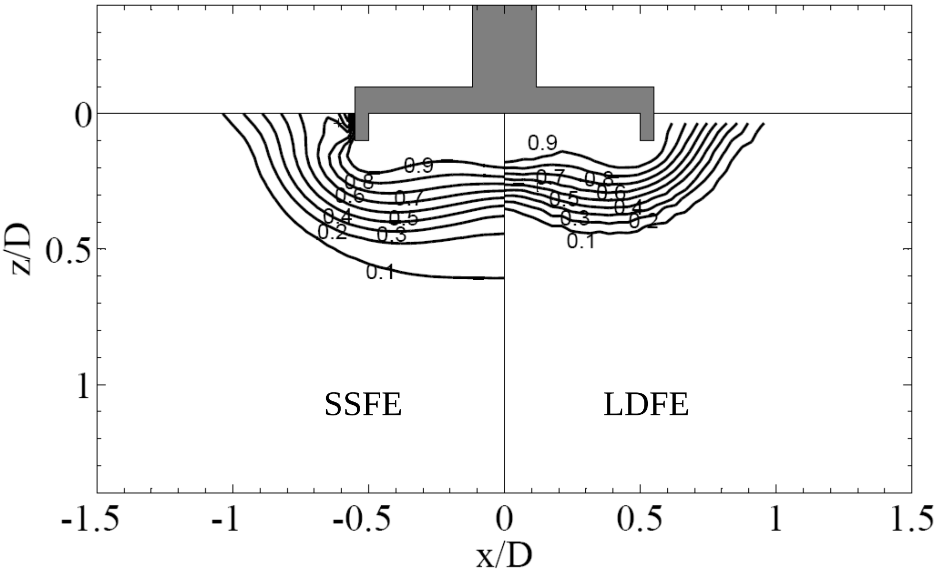

(b) Uplift

Fig. 8. Comparison of failure mechanisms predicted by SSFE and LDFE analyses (d/D = 0.1): (a) Compression; (b) Uplift